EPJ Web of Conferences **36**, 00009 (2012)
DOI: 10.1051/epjconf/20123600009

Hadronic resonances from ALICE in pp collisions

Enrico Fragiacomo (for the ALICE Collaboration)[1,a]

[1]INFN - Sezione di Trieste
Via Valerio 2, 34127 Trieste, Italy

Abstract. The study of resonances in $\sqrt{s} = 7$ TeV pp collisions provides a test of QCD in a new energy domain as well as a baseline for heavy-ion collisions. The resonances $K^*(892)^0$, $\phi(1020)$, $\Sigma(1385)^{\pm}$, $\Lambda(1520)$, and $\Xi(1530)^0$ have been reconstructed at mid-rapidity from their hadronic decay using data collected by the ALICE detector. The comparison of $\phi(1020)$ and $\Sigma(1385)$ p_T-spectra to QCD-inspired models such as PHOJET and different PYTHIA tunes are shown.

1 Introduction

Resonance production is an important issue both in pp and in heavy-ion collisions. In pp collisions, it contributes to the understanding of hadron production [1] as the decay products of resonances represent a large fraction of the final state particles, and it provides a reference for tuning QCD-inspired event generators. In heavy-ion collisions, due to their short lifetime (few fm/c), resonances can both decay and be regenerated by final state interactions inside the hot and dense matter region and therefore are sensitive to its dynamical evolution [2–4].

The hadronic resonances, $K^*(892)^0$, $\phi(1020)$, $\Sigma(1385)^{\pm}$, $\Lambda(1520)$ and $\Xi(1530)^0$, have been measured with the ALICE experiment in pp collisions at the center of mass energy of $\sqrt{s} = 7$ TeV. Data analysis was carried out at mid-rapidity ($|y| < 0.5$ for $K^*(892)^0$ and $\phi(1020)$, $|y| < 0.8$ for $\Sigma(1385)$, $\Lambda(1520)$ and $\Xi(1530)^0$) on a sample of minimum-bias events collected by ALICE during the CERN LHC run in 2010.

In section 2 a brief introduction of the detector characteristics which affect this analysis is presented. Tracking and particle identification are discussed. In section 3 the analysis is described with emphasis on the signal extraction. In section 4 the transverse momentum spectra for $\phi(1020)$ and $\Sigma(1385)$ are compared to two QCD based event generators, PHOJET [5] and PYTHIA [6]. An agreement between data and models is observed only in a limited region of p_T. Finally, in section 6 the ratios ϕ/K^- and ϕ/π^- are calculated with the yield of pions and kaons previously measured with the ALICE detector [8]. The ratios are compared with previous measurements at lower energies. Conclusions are drawn in section 7.

2 Experimental setup

The ALICE detector is described in detail in [9,10]. For the analysis described in this paper, only the central barrel has been used. The central tracking and PID detectors, covering a pseudo-rapidity window of $|\eta| < 0.9$, include, from the innermost outwards, the Inner Tracking System (ITS), the Time Projection Chamber (TPC) and the Time of Flight array (TOF). The central detectors are embedded in a 0.5 T solenoidal field. The moderate field, together with a low material budget permits the reconstruction of low p_T tracks.

[a] e-mail: enrico.fragiacomo@ts.infn.it

The ITS is composed of six layers of silicon detectors. The two innermost layers, based on silicon pixels (SPD), are also used in the on-line trigger. The four outer layers, made of drift and strip detectors, provide identification via the specific energy loss with a 10% resolution.

The TPC [11] provides track reconstruction with up to 159 three-dimensional space points per track in a cylindrical active volume of about 90 m^3. In order to ensure high efficiency and good dE/dx resolution and to keep low the contamination from secondaries and fakes, tracks were required to have at least 70 reconstructed clusters in the TPC. In order to improve the global resolution, tracks were accepted only in the range $|\eta| < 0.8$ (i.e. well within the TPC acceptance) and with $p_T \geq 0.15$ GeV/c.

The standard tracking used in this analysis combines the information from the ITS and TPC. It provides very good resolution in the distance of closest approach to the vertex, and hence better separation of primary and secondary particles.

The TPC identifies particles via the specific energy loss dE/dx with a 5.2% resolution [11]. This is achieved calculating the difference between the measured energy loss and the one expected for different mass hypotheses. The cut on this difference, normalized to the resolution σ_{TPC}, is optimized for each analysis and depends in general on the signal to background ratio and on the transverse momentum. The TPC dE/dx measurements allow pions to be separated from kaons for momenta up to $p \sim 0.7$ GeV/c, while the proton/antiproton band starts to overlap with the pion/kaon band at $p \sim 1$ GeV/c. The electron/positron dE/dx crosses the other bands at various momenta, see figure 1, left.

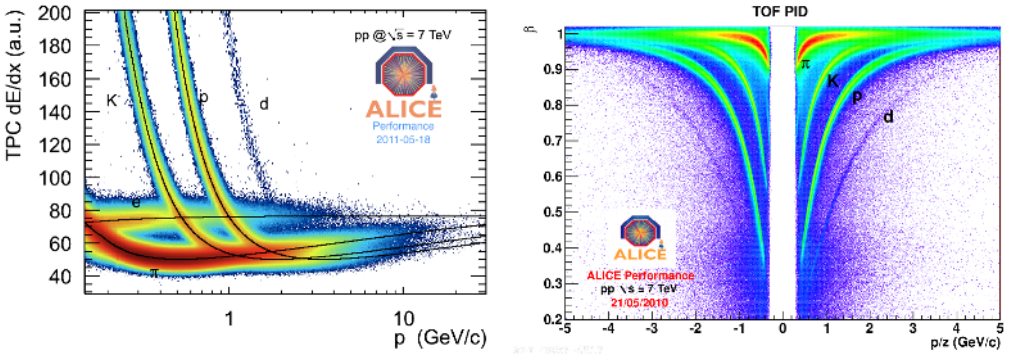

Fig. 1. Left: Specific ionization energy loss dE/dx vs. momentum for tracks measured with the ALICE TPC. The solid lines are parametrizations of the Bethe-Bloch curve [12]. Right: Velocity β of particles measured by the TOF vs. momentum.

Placed at a radius of 370-399 cm, the TOF measures the time-of-flight of the particles, allowing identification at higher p_T. Particles which reach the TOF detector are identified by the correlation between their momentum and their velocity $\beta = L/ct$, where L is the total integrated path length and t is the measured time of flight (see figure 1, right). Particles are identified by the difference between the measured time-of-flight and the one expected from a given particle (π, K, p). With a total time resolution of about 120 ps, pions can be separated from kaons up to $p \sim 2.0$ GeV/c and the two mesons can be distinguished from (anti)protons up to $p \sim 2.5$ GeV/c.

3 Analysis

The data analysis is carried out using a sample of minimum-bias pp data collected by ALICE during 2010, with a size ranging from 60 to 155 million events, for the different resonances analyzed. The sample is corrected for trigger inefficiencies and biases to recover a normalized sample of inelastic (INEL) events. The events are selected within 10 cm of the detector's center along the beam direction, with vertex resolution in the transverse plane of a few hundred micrometers. The event vertex range

is selected to maximize particle trajectory (track) reconstruction efficiency within the ITS and TPC volume.

The resonances have been identified via their main decay channel: $K^*(892)^0 \longrightarrow \pi^{\pm}+K^{\mp}$, $\phi(1020) \longrightarrow K^+ + K^-$, $\Sigma(1385)^{\pm} \longrightarrow \Lambda + \pi^{\pm}$, $\Lambda(1520) \longrightarrow p + K^-$ and $\Xi(1530)^0 \longrightarrow \Xi^- + \pi^+$.

Due to their very short lifetime, resonance decay products cannot be distinguished from the particles coming from the primary vertex, and their yield can only be measured by first computing the invariant mass spectrum of all primary candidate tracks and then subtracting the combinatorial background.

For both the $\phi(1020)$ and the $\Xi(1530)^0$ the invariant mass distributions were fitted with a function composed of a polynomial to describe the background, plus a Voigtian, i.e. the convolution of a Gaussian and a Breit-Wigner (see figure 2 for given p_T bins as example). This was done to account for the resolution in the invariant mass which ranges between 1 and 2 MeV/c^2 and is therefore comparable with the nominal widths of the resonances (4.25 and 9.1 MeV/c^2, respectively [13]).

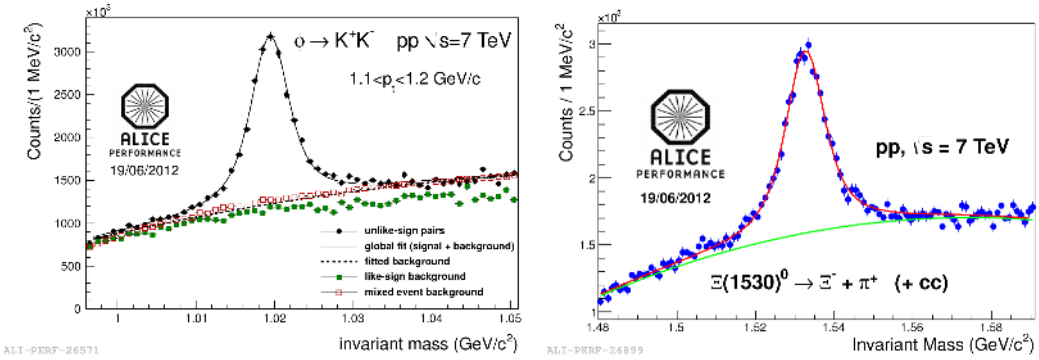

Fig. 2. Combined fit to the invariant mass distribution for the $\phi(1020)$ (left) and the $\Xi(1530)^0$ (right). The fitting function is the sum of a polynomial and a Voigtian. For the $\phi(1020)$ the fitted background is compared with the background evaluated with other techniques (mixing events and like-sign).

In both cases, one parameter, namely the Gaussian standard deviation σ for the $\phi(1020)$ and the Breit-Wigner width Γ for the $\Xi(1530)^0$, was kept fixed to help the convergence of the fit. The Breit-Wigner width Γ for the $\Xi(1530)^0$ was fixed to the PDG value from [13]. Table 1 summarizes the results of the fitting procedure. In both cases the masses, i.e. the mean values of the Breit-Wigner signal functions, are compatible within errors with the corresponding PDG values from [13].

Table 1. Masses and widths compared to the PDG values (experimental uncertainties are statistical only). Note that for the $\Sigma(1385)$ the PDG average between $\Sigma(1385)^+$ and $\Sigma(1385)^-$ has been considered.

	p_T-bin (GeV/c)	Mass (MeV/c^2)	PDG Mass	Γ (MeV/c^2)	PDG Γ	σ (MeV/c^2)
$K^*(892)^0$	2.0-2.5	893.4 ± 0.5	895.9	54.0 ± 2.0	48.7	-
$\phi(1020)$	0.7-0.8	1019.30 ± 0.10	1019.46	4.52 ± 0.5	4.26	fixed to 1.0
$\Sigma(1385)$	1.6-1.8	1383 ± 1	1385.0	33 ± 3	37.6	-
$\Xi(1530)^0$	1.2-1.6	1531.5 ± 0.4	1531.8	fixed to PDG	9.1	2.0 ± 0.5

Alternative methods, like the event-mixing and the like-sign, have been employed with comparable success for the description of the combinatorial background. For event-mixing, to assure a similar event structure, tracks from events with similar vertex positions z ($\Delta z < 1$ cm) and track multiplicities n ($\Delta n < 10$) were mixed.

For the Σ(1385) the invariant mass was fitted with a function consisting of a negative power-law polynomial for the background and a Gaussian. An example is shown in figure 3 for all the four Σ(1385) species together ($\Sigma(1385)^+$, $\Sigma(1385)^-$ and corresponding antiparticles). The values for the mass and the width (FWHM=2.35σ) from the fit are shown in table 1. Note that both the mass and the width are compatible within the errors with the averaged PDG values for $\Sigma(1385)^+$ and $\Sigma(1385)^-$.

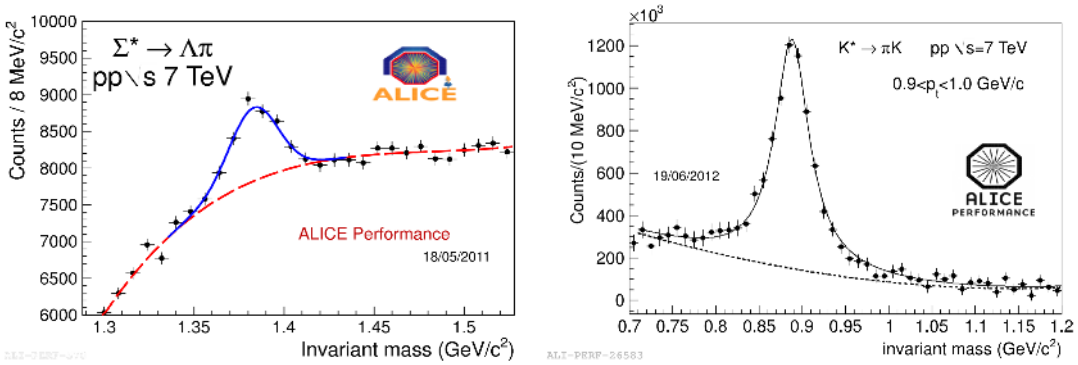

Fig. 3. Left: Combined fit to the invariant mass distribution for the Σ(1385). The fitting function (in blue) is the sum of a negative power-law polynomial and a Gaussian. Right: Combined fit to the invariant mass distribution after like-sign background subtraction for the $K^*(892)^0$. A polynomial is added to the Breit-Wigner to account for the residual background. In both case, the background (residual background for the $K^*(892)^0$) from the fit is drawn with a dashed curve.

For the $K^*(892)^0$ the like-sign method turned out to produce better results than the event-mixing technique and was therefore employed for the determination of the background. After the like-sign background is subtracted, a residual background remains. This is due in part to an imperfect description of the combinatorial background but mainly caused by a real correlated background. The latter can arise from correlated πK pairs or from misidentified particle decays (for example, ϕ and ρ, or from underlying jet event structure). In order to account for the residual background, a polynomial has been added to the Breit-Wigner signal fitting function. An example, for the p_T-bin between 0.9 and 1.0 GeV/c, is presented in figure 3 and the results of the fit are shown in table 1.

The Λ(1520) background has been described by an event-mixing technique and subtracted from the invariant mass distribution. An example, for the p_T-bin 1.0-1.25 GeV/c, is shown in figure 4. The combinatorial background has been arbitrarily normalized to the data in the region between 1.6 and 1.7 GeV/c^2.

For all the resonances, the raw counts, obtained integrating the signal functions, are corrected for the detector efficiency and the acceptance using PYTHIA Perugia 0 [14] generated Monte Carlo events propagated through ALICE using GEANT3 [15].

Two types of systematic uncertainties in the resulting particle spectra have been considered: p_T-dependent systematic uncertainties, which are due to the efficiency determination and the signal quality at a given p_T, and the p_T-independent uncertainties due to normalization and other factors. The main point-to-point contributions come from the signal extraction (±2-10% for the ϕ(1020) and ±8-15% for the Σ(1385)) and from the tracking efficiency (±8% for both particles), while the INEL normalization leads to a +7.0% and -3.5% (p_T-independent) uncertainty on the yield for all measured particles.

4 Results

The transverse momentum spectrum of the ϕ(1020) [7] is shown in figure 5 and compared with the spectrum of the ϕ(1020) from the analysis of ALICE data at $\sqrt{s}$ = 900 GeV [8]. Note that the yields

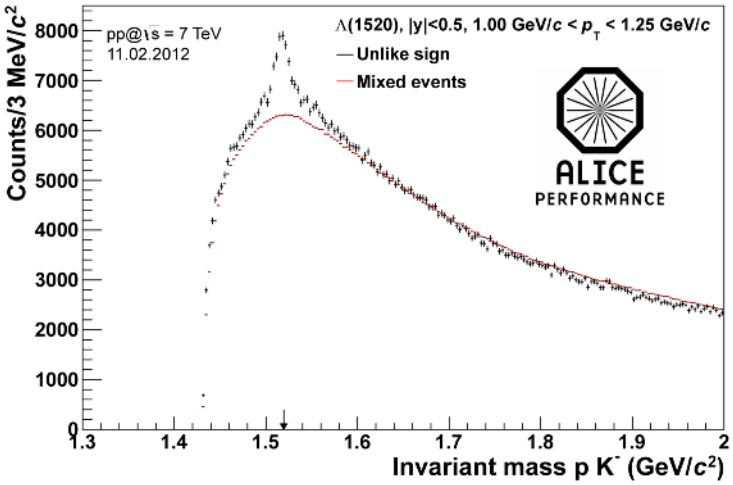

Fig. 4. Invariant mass distribution for the Λ(1520). The background (in red) has been evaluated via event mixing technique.

scale with the multiplicity of the collision. Both spectra are fitted with a Lévy-Tsallis function [19]

$$\frac{\mathrm{d}^2N}{\mathrm{d}y\mathrm{d}p_{\mathrm{T}}} = \frac{(n-1)(n-2)}{nT[nT+m(n-2)]} \times \frac{\mathrm{d}N}{\mathrm{d}y} \times p_{\mathrm{T}} \times \left(1+\frac{m_{\mathrm{T}}-m}{nT}\right)^{-n} \quad (1)$$

where $m_{\mathrm{T}} = \sqrt{m^2+p_{\mathrm{T}}^2}$. This function describes both the exponential shape of the spectrum at low p_{T} and the power-law distribution at large p_{T}, quantified by the inverse slope parameter T and the exponent parameter n, respectively. Table 2 show the results of the fit. The extracted n value is similar to the one quoted by STAR for the $\phi(1020)$ measured in pp collisions at 200 GeV (n = 8.3 ± 1.2) [4]. In contrast, the slope parameter is significantly higher than the value obtained at RHIC, T = 202 ± 14 ± 11 MeV. From the Lévy-Tsallis function the mean transverse momentum <p_{T}> has been

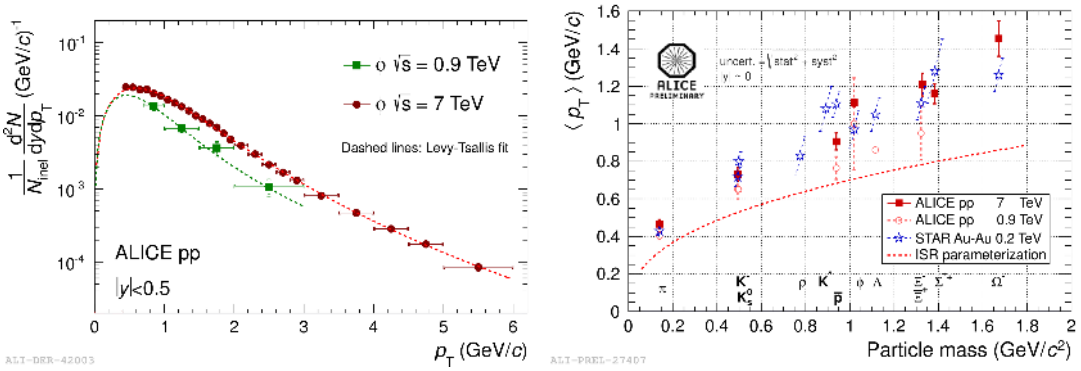

Fig. 5. Left: Transverse momentum spectra for the $\phi(1020)$ [7] fitted with a Lévy-Tsallis function. The data at $\sqrt{s}$ = 900 GeV are from a previous analysis [8]. Note that for the data at $\sqrt{s}$ = 7 TeV the uncertainties are smaller than the symbol size. Right: <p_{T}> vs. particle mass.

Table 2. Parameters extracted from the Lévy-Tsallis (1) fits to the transverse momentum spectra, including point-to-point systematic uncertainties. For the 7 TeV points, the first uncertainty is statistical and the second is systematic.

$\sqrt{s}$ (TeV)	T (MeV)	n	χ^2/NDF
0.9	164 ± 91	4.2 ± 2.5	0.6/1
7	272 ± 4 ± 11	6.7 ± 0.20 ± 0.4	2.8/23

also estimated. The $<p_T>$ is shown in figure 5 (right), as a function of the particle mass and compared with the value at 900 GeV from ALICE [8]. The mean p_T is in agreement with the trend drawn by other particles at 7 TeV from ALICE, which in turn differs from the ISR parametrization of values from lower energy experiments. The trend of ALICE points at 7 TeV in pp collisions is comparable to the STAR values at 200 GeV in Au–Au collisions from STAR [2,4] (also shown in figure 5).

5 Comparison to models

The transverse momentum spectra of $\phi(1020)$ and $\Sigma(1385)$ are compared to PHOJET and various PYTHIA tunes in figure 6. For PYTHIA, tunes D6T (109), ATLAS-CSC (306), Perugia0 (320) and Perugia-2011 (350) were used.

For the $\phi(1020)$ the best agreement is found for the PYTHIA Perugia-2011 tune, which reproduces the high-p_T part ($p_T > 3$ GeV/c) of the $\phi(1020)$ spectrum rather well. PHOJET and ATLAS-CSC very significantly overestimate the low-momentum part ($p_T < 1$ GeV/c) of the transverse momentum distribution but reproduce the high-momentum distribution. The PYTHIA D6T tune is only able to describe the low-p_T part ($p_T < 2$ GeV/c) of the $\phi(1020)$ spectrum. Finally, the PYTHIA Perugia0 tune underestimates the meson yields for all transverse momenta.

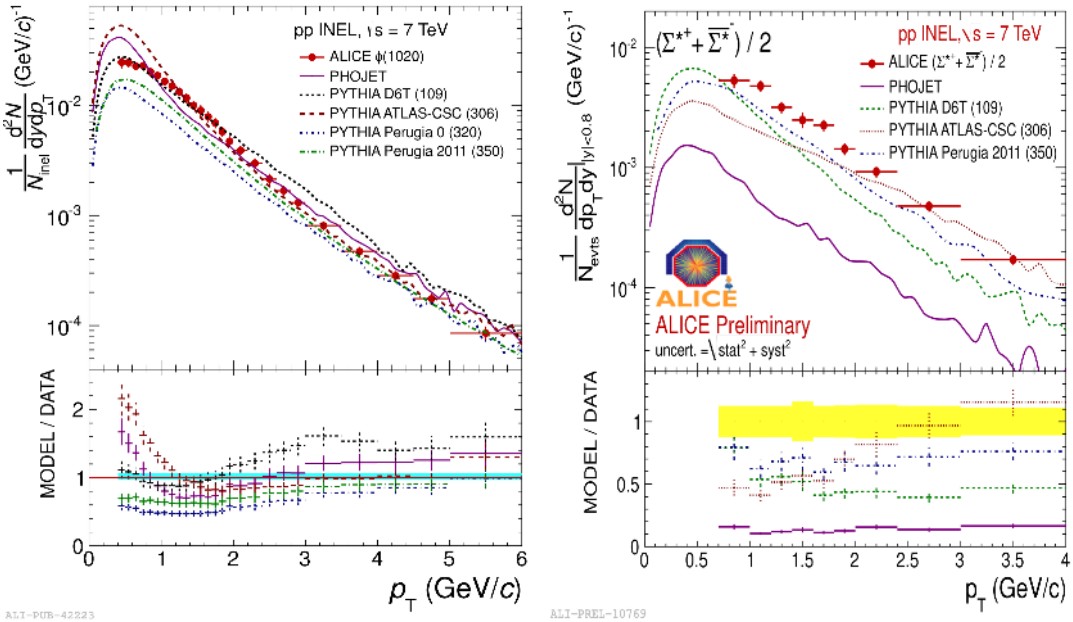

Fig. 6. The transverse momentum spectra of $\phi(1020)$ (left) and $\Sigma(1385)^+$ (right) are compared to PHOJET and various PYTHIA tunes (D6T (109), ATLAS-CSC (306), Perugia0 (320) and Perugia-2011 (350)). The colored bands indicates the uncertainties.

For the Σ(1385) all the models seem to underestimate the data, with only a fair agreement for ATLAS-CSC at high p_{T} (> 2 GeV/c).

6 Particle ratios

Using the $\phi(1020)$ yields presented in this paper and stable particle results measured with ALICE at the same energy [20], we find the following values for particle ratios in pp collisions at 7 TeV: $\phi/\mathrm{K}^- = 0.12 \pm 0.001$ (stat.) $\pm$ 0.02 (syst.), $\phi/\pi^- = 0.014 \pm 0.0002$ (stat.) $\pm$ 0.002 (syst.). These ratios are shown in figures 7 together with the results obtained at lower incident energies in pp, $\mathrm{e}^+\mathrm{e}^-$, and A–A collisions.

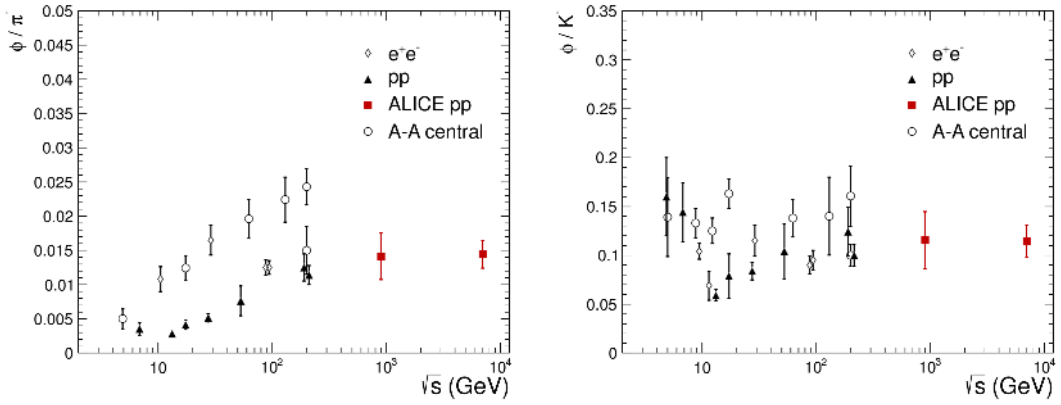

Fig. 7. Energy dependence of the ϕ/π^-(left) and ϕ/K ratio (right) in nuclear (triangles) [4,21–24,28,25] and pp (squares) [4,22,2,25,26,29,30] collisions. Diamonds represent the ALICE data at 0.9 and 7 TeV. The pion yields at 7 TeV are from [20]. The $\phi(1020)$, π, and K yields at 0.9 TeV are from [27,31].

The ϕ/K ratio is essentially independent of energy and also independent of the collision system. On the contrary, the ϕ/π ratio increases with energy both in heavy-ion and in pp collisions up to at least 200 GeV.

7 Conclusions

The hadronic resonances $\mathrm{K}^*(892)^0$, $\phi(1020)$, $\Sigma(1385)^{\pm}$, $\Lambda(1520)$ and $\Xi(1530)^0$ have been measured with the ALICE experiment in pp collisions at an energy in the center of mass of $\sqrt{s} = 7$ TeV. Several methods for the raw yield extraction have been discussed and the values for the masses and the widths have been compared to the PDG values.

The transverse momentum spectra for the $\phi(1020)$ and Σ(1385) have been presented. A Lévy-Tsallis function well describes the spectra. The yields of the $\phi(1020)$ have been compared to a previous measurement performed with ALICE at 900 GeV, showing an increase which scales with the multiplicity of the collisions. The average p_{T} increases by about 30% with respect to previous measurements at lower energies.

The ϕ/K ratio is found to stay independent of energy up to 7 TeV. Also the ϕ/π ratio, which increases in both pp and A–A collisions up to at least RHIC energies, saturates and becomes independent of energy above 0.2 TeV.

The data have been compared to a number of PYTHIA tunes and the PHOJET event generator. None of them gives a fully satisfactory description of the data. The latest PYTHIA version (Perugia-2011) comes closer while still under predicting the $\phi(1020)$ meson p_{T}-spectrum below 3 GeV/c by up to a factor of two.

References

1. M. Aguilar-Benitez et al. (LEBC-EHS Collaboration) , Z. Phys. C **50** (1991) 405.
2. J. Adams et al. (STAR Collaboration), Phys. Rev. C **71** (2005) 064902.
3. S.S. Adler et al. (PHENIX Collaboration), Phys. Rev. C **72** (2005) 014903.
4. B.I. Abelev et al. (STAR Collaboration), Phys. Rev. C **79** (2009) 064903.
5. R. Engel et al., Z. Phys. C **66** (1995) 203; R. Engel and J. Ranft, Phys. Rev. D **54** (1996) 4244.
6. T. Sjöstrand, S. Mrenna and P. Skands, J. High Energy Phys. **05** (2006) 026.
7. B. Abelev et al. (ALICE Collaboration), accepted for publication by Eur. Phys. J. C., arXiv::1208.5717v2
8. K. Aamodt et al. (ALICE Collaboration), Eur. Phys. J. C. (2011) 71
9. K. Aamodt et al. (ALICE Collaboration), J. Instrum. **3** (2008) S08002.
10. K. Aamodt et al. (ALICE Collaboration), J. Instrum. **5** (2010) P03003.
11. J. Alme et al., Nucl. Instr. Meth. in Phys. Res. A **622** (2010) 316.
12. W. Blum, W. Riegler, and L. Rolandi, *Particle Detection with Drift Chambers*, 2nd ed. (Springer Verlag, 2008).
13. K. Nakamura et al., J. Phys. G **37** (2010) 075021.
14. P.Z. Skands, Phys. Rev. D 82 (2010) 074018, arXiv:1005.3457v4, http://dx.doi.org/10.1103/PhysRevD.82.074018.
15. R. Brun, F. Carminati, S. Giani, GEANT detector description and simulation tool, CERN-W5013.
16. H. Albrecht et al., Z. Phys. C**61** (1994) 1.
17. F. Becattini, M. Gazdzicki, J. Solfrank, Eur. Phys. J. C **5** (1998) 143.
18. N. Armesto et al., J. Phys. G. Nucl. Part. Phys. **35** (2008) 054001.
19. C. Tsallis, J. Stat. Phys. **52** (1988) 479.
20. M. Chojnacki (ALICE Collaboration), Proc. of Quark Matter 2011, Annecy, France.
21. B.B. Back et al., (E917 Collaboration), Phys. Rev. C **69** (2004) 054901.
22. S.V. Afanasiev et al. (NA49 Collaboration) Phys. Lett. B **491** (2000) 59.
23. C. Adler et al. (STAR Collaboration) Phys. Rev. C **65** (2002) 041901.
24. K. Adcox et al. (PHENIX Collaboration) Phys. Rev. Lett. **88** (2002) 242301.
25. J. Adams et al. (STAR Collaboration), Phys. Rev. Lett. **92** (2004) 112301.
26. V. Blobel et al., Phys. Lett. **B59** (1975) 88.
27. K. Aamodt et al. (ALICE Collaboration), Eur. Phys. J. C **71** (2011) 1594.
28. J. Adams et al. (STAR Collaboration), Phys. Lett. B **612** (2005) 181.
29. C. Daum et al., Nucl. Phys. B **186** (1981) 205.
30. A.M. Rossi et al., Nucl. Phys. B **84** (1975) 269.
31. K. Aamodt et al. (ALICE Collaboration), Eur. Phys. J. C **71** (2011) 1655.
32. V.V. Anisovich and M.N. Kobrinsky, Phys. Lett. B **52** (1974) 217.